AFRL-PR-WP-TP-2006-273

DIODE LASER SENSOR FOR GAS TEMPERATURE AND H_2O CONCENTRATION IN A SCRAMJET COMBUSTOR USING WAVELENGTH MODULATION SPECTROSCOPY (POSTPRINT)

Gregory B. Rieker, Jonathan T.C. Liu, Jay B. Jeffries, Ronald K. Hanson, Tarun Mathur, Mark R. Gruber, and Campbell D. Carter

JULY 2005

Approved for public release; distribution is unlimited.

STINFO COPY

© 2005 by the nongovernment authors.
The U.S. Government is joint author of the work and has the right to use, modify, reproduce, release, perform, display, or disclose the work.

PROPULSION DIRECTORATE
AIR FORCE MATERIEL COMMAND
AIR FORCE RESEARCH LABORATORY
WRIGHT-PATTERSON AIR FORCE BASE, OH 45433-7251

REPORT DOCUMENTATION PAGE

Form Approved
OMB No. 0704-0188

The public reporting burden for this collection of information is estimated to average 1 hour per response, including the time for reviewing instructions, searching existing data sources, searching existing data sources, gathering and maintaining the data needed, and completing and reviewing the collection of information. Send comments regarding this burden estimate or any other aspect of this collection of information, including suggestions for reducing this burden, to Department of Defense, Washington Headquarters Services, Directorate for Information Operations and Reports (0704-0188), 1215 Jefferson Davis Highway, Suite 1204, Arlington, VA 22202-4302. Respondents should be aware that notwithstanding any other provision of law, no person shall be subject to any penalty for failing to comply with a collection of information if it does not display a currently valid OMB control number. **PLEASE DO NOT RETURN YOUR FORM TO THE ABOVE ADDRESS**.

1. REPORT DATE *(DD-MM-YY)*	2. REPORT TYPE	3. DATES COVERED *(From - To)*
July 2005	Conference Paper Postprint	09/01/2004 – 07/31/2005

4. TITLE AND SUBTITLE

DIODE LASER SENSOR FOR GAS TEMPERATURE AND H_2O CONCENTRATION IN A SCRAMJET COMBUSTOR USING WAVELENGTH MODULATION SPECTROSCOPY (POSTPRINT)

5a. CONTRACT NUMBER
In-house

5b. GRANT NUMBER

5c. PROGRAM ELEMENT NUMBER
62203F

6. AUTHOR(S)

Gregory B. Rieker, Jonathan T.C. Liu, Jay B. Jeffries, and Ronald K. Hanson, (Stanford University)
Tarun Mathur (Innovative Scientific Solutions, Inc.)
Mark R. Gruber and Campbell D. Carter (AFRL/PRAS)

5d. PROJECT NUMBER
3012

5e. TASK NUMBER
AI

5f. WORK UNIT NUMBER
00

7. PERFORMING ORGANIZATION NAME(S) AND ADDRESS(ES)

Stanford University
High Temperature Gasdynamics Laboratory
Department of Mechanical Engineering
Stanford, CA, 94305

Innovative Scientific Solutions, Inc.
Dayton, OH, 45433

Propulsion Sciences Branch (AFRL/PRAS)
Aerospace Propulsion Division
Propulsion Directorate
Air Force Research Laboratory
Air Force Materiel Command
Wright-Patterson AFB, OH 45433-7251

8. PERFORMING ORGANIZATION REPORT NUMBER
AFRL-PR-WP-TP-2006-273

9. SPONSORING/MONITORING AGENCY NAME(S) AND ADDRESS(ES)

Propulsion Directorate
Air Force Research Laboratory
Air Force Materiel Command
Wright-Patterson AFB, OH 45433-7251

10. SPONSORING/MONITORING AGENCY ACRONYM(S)
AFRL-PR-WP

11. SPONSORING/MONITORING AGENCY REPORT NUMBER(S)
AFRL-PR-WP-TP-2006-273

12. DISTRIBUTION/AVAILABILITY STATEMENT
Approved for public release; distribution is unlimited.

13. SUPPLEMENTARY NOTES
Conference paper published in the 41st AIAA/ASME/SAE/ASEE Joint Propulsion Conference & Exhibit (2005).

© 2005 by the nongovernment authors. The U.S. Government is joint author of the work and has the right to use, modify, reproduce, release, perform, display, or disclose the work. PAO Case Number: AFRL/WS 06-2362; Date cleared: 04 Oct 2006. Paper contains color.

14. ABSTRACT

A diode laser absorption sensor which probes three spectral features of water vapor in the near infrared region to infer gas temperature and water vapor concentration near the exit of a scramjet combustor is presented. Optical engineering is used to overcome beam steering and fiber mode noise sources. A method to make absolute measurements using wavelength modulation spectroscopy (WMS) with second harmonic detection ($2f$) is described, along with the advantages of the technique over direct absorption spectroscopy. Measurements using both techniques in the scramjet combustor are compared to show superior noise rejection and overall signal to noise ratios with WMS-$2f$. Results of temperature and water vapor partial pressure under various scramjet operating conditions show the utility of the sensor for scramjet engine design and optimization.

15. SUBJECT TERMS
Supersonic combustion, fuel injection, laser-based diagnostics

16. SECURITY CLASSIFICATION OF:			17. LIMITATION OF ABSTRACT:	18. NUMBER OF PAGES	19a. NAME OF RESPONSIBLE PERSON (Monitor)
a. REPORT	b. ABSTRACT	c. THIS PAGE			Mark R. Gruber
Unclassified	Unclassified	Unclassified	SAR	18	19b. TELEPHONE NUMBER *(Include Area Code)* N/A

Standard Form 298 (Rev. 8-98)
Prescribed by ANSI Std. Z39-18

41st AIAA/ASME/SAE/ASEE Joint Propulsion Conference & Exhibit
10 - 13 July 2005, Tucson, Arizona

AIAA 2005-3710

Diode Laser Sensor for Gas Temperature and H_2O Concentration in a Scramjet Combustor Using Wavelength Modulation Spectroscopy

Gregory B. Rieker [*], Jonathan T.C. Liu [*], Jay B. Jeffries[†], Ronald K. Hanson[‡]
High Temperature Gasdynamics Laboratory
Department of Mechanical Engineering
Stanford University, Stanford, CA, 94305

Tarun Mathur[§]
Innovative Scientific Solutions, Inc
Dayton, OH, 45433

and

Mark R. Gruber[**], Campbell D. Carter[**]
Air Force Research Laboratory (AFRL/PRAS)
Wright-Patterson Air Force Base
Dayton, OH, 45433

A diode laser absorption sensor which probes three spectral features of water vapor in the near infrared region to infer gas temperature and water vapor concentration near the exit of a scramjet combustor is presented. Optical engineering is used to overcome beam steering and fiber mode noise sources. A method to make absolute measurements using wavelength modulation spectroscopy (WMS) with second harmonic detection (2*f*) is described, along with the advantages of the technique over direct absorption spectroscopy. Measurements using both techniques in the scramjet combustor are compared to show superior noise rejection and overall signal to noise ratios with WMS-2*f*. Results of temperature and water vapor partial pressure under various scramjet operating conditions show the utility of the sensor for scramjet engine design and optimization.

I. Introduction

Recent successful tests of scramjet engine powered test vehicles at velocities in excess of Mach 9 have illustrated the potential of this technology as an option for high-speed air-breathing flight. At the heart of these high speed vehicles is the combustor, the region in which a supersonic air/fuel mixture ignites and burns to produce thrust. The health of the combustor plays a major role in the stability and efficiency of the engine, and can be determined by looking at important gasdynamic parameters in the post-combustion effluent. In the work reported here, a tunable diode laser (TDL) sensor is developed and ground test measurements made in the exhaust of a model scramjet combustor at the Air Force Research Laboratory.

There has been significant recent progress to develop practical sensors for aero-engine ground test based on telecommunications TDLs.[1-5] These hardy, fiber-coupled devices can be rapidly tuned in wavelength, multiplexed into a single optical beam, and directed across a selected path in the inlet, combustor, or exhaust of an engine. When the device is tuned across an atomic or molecular absorption feature, several spectroscopic techniques can be used to infer path-integrated gas properties such as temperature, species concentration, pressure or velocity.

[*] PhD student, Stanford University, AIAA Student Member
[†] Senior Research Engineer, Stanford University, AIAA Associate Fellow
[‡] Professor, Stanford University, AIAA Fellow
[§] Senior Research Engineer, Innovative Scientific Solutions, AIAA Member
[**] Senior Aerospace Engineer, AFRL/PRAS, AIAA Associate Fellow

Copyright © 2005 by the authors. Published by the American Institute of Aeronautics and Astronautics, Inc., with permission.

Traditionally, scanned-wavelength direct absorption spectroscopy has been the technique of choice for aero-engine applications because of its simplicity, accuracy, and ability to make absolute measurements. In harsh combustion environments such as the scramjet, however, the technique can suffer from low signal-to-noise ratios arising from mechanical and gasdynamic beam steering, weak absorption at high temperatures, and fiber mode noise.[4] The scanned-direct absorption technique must rely entirely on careful optical engineering to reduce noise to acceptable levels. Another technique which has recently been explored for its increased sensitivity to small signals and ability to reject noise is wavelength modulation spectroscopy (WMS) with second harmonic detection (2*f*). This technique, often simply referred to as WMS-2*f*, employs a lock-in amplifier to isolate the second harmonic of the detected signal, greatly enhancing the noise rejection characteristics. Thus far, the technique has only been applied to practical combustion applications to make *relative* measurements of gas properties, and required calibration using another technique (generally direct absorption).[5,22-24] This paper will explore the use of WMS-2*f* as a means to make *absolute* measurements of temperature and gas concentration. Example signal-to-noise ratio (SNR), temperature, and fast-Fourier transform (FFT) data obtained in a scramjet combustor using both scanned-direct absorption and WMS-2*f* under nearly identical operating conditions will be compared to illustrate the benefits of WMS-2*f* in harsh environments. In addition, temperature and water vapor partial pressure results under varying engine conditions will be used to demonstrate the usefulness of the sensor as a diagnostic tool for engine developers.

II. Sensor Architecture

A. Optical Hardware

The sensor utilizes a beam of infrared light consisting of the multiplexed output of four TDLs. The light is pitched across the combustor exit plane, collected, and dispersed onto four separate detectors. Three of the lasers are wavelength-scanned across H_2O transitions and used to infer the static temperature via two spectroscopic techniques (discussed in section IID). The fourth laser is fixed at a non-resonant wavelength to detect transmission perturbations from gasdynamic or mechanical beam steering, window fouling, or particulates in the flow.

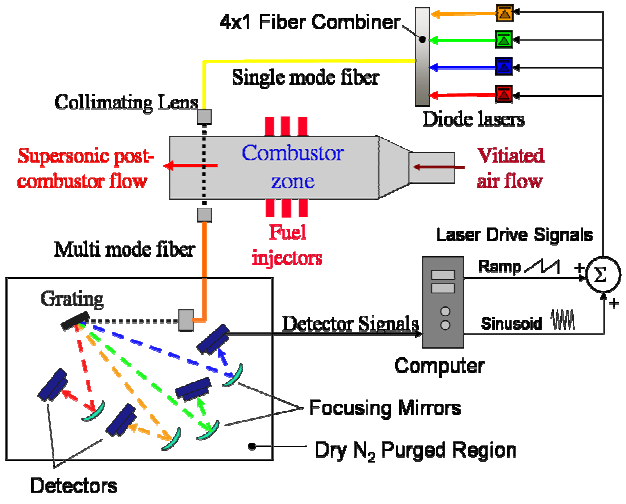

Figure 1. Schematic of optical setup.

A schematic of the optical arrangement of the sensor is shown in Fig. 1. Four fiber-coupled DFB diode lasers (NEL America, Inc.) are multiplexed with a 9-micron single-mode fiber combiner. A 10-meter single-mode fiber delivers the beam to the scramjet test section, where it is pitched across the combustor exit with an aspheric collimating lens (Thorlabs F230FC-C). After traversing the test region, the beam is collected with a large diameter lens (Oz Optics HPUCO-25-1300-M-10BQ), and focused into a 400 micron multimode fiber. The beam travels through the multimode fiber to a demultiplexing setup a few meters from the test section. The light exits the multimode fiber and is collimated by a large diameter aspheric lens (Optosigma 023-2392) onto a 30 mm square, 1200 grooves/mm diffraction grating (Edmund Optics NT43-852). The dispersed light beams are focused onto separate 3mm diameter InGaAs photodetectors (Electro-Optical Systems Inc., IGA-030-E5/4MHz).

This optical arrangement represents a vast improvement over previous optical designs.[4] The primary sources of noise that are addressed with the current design are beam steering and fiber mode noise. Beam steering, which is caused by mechanical vibration and refraction of the beam by rapidly changing density gradients in the supersonic flow, is suppressed by the large collimating lens and 400 micron fiber. These components outperform smaller optics by maintaining beam focus on the multimode fiber through a greater degree of axial and radial beam misalignment. Fiber mode noise is a wavelength-dependent spatial variation of light intensity across the core of a multimode fiber. It can cause rapid fluctuations in the detected signal strength if the light beam is not entirely collected by the photodetector. To combat the effects of fiber mode noise, the multimode fiber length is kept to a minimum and large area detectors are employed to collect the largest possible fraction of each dispersed beam.

All laser drive signal generation and detector output acquisition is performed by one computer running Labview software. The inputs and outputs are routed through two National Instruments multi-function DAQ cards (PCI-

6115). Using the computer for laser drive signal generation provides virtually limitless options of signal form, and allows for easy, on-the-fly variation for different types of spectroscopy. The detector output signals are recorded and saved raw without any processing (baseline fitting, lock-in amplifier, etc.). This allows post-processing of the data using several different methods, including methods not yet considered at the time of the measurement campaign. For the WMS-2*f* experiments of this work, new methods of data reduction were investigated after the campaign.

B. Scramjet Test Facility

The scramjet test facility at Wright-Patterson Air Force Base in Dayton, Ohio will not be covered in detail here because an in-depth treatment is available in the literature.[6-9] A schematic of the facility is shown in Fig. 2. Approximate gas properties and important inflows are shown in the block diagram above the schematic. Compressed air is supplied to the scramjet test facility at 13.6 kg/s and up to 920 K and 5.2 MPa. The air enters a vitiator where fuel is injected and combusted to raise the gas temperature and pressure. Make-up oxygen replaces that which is burned in the vitiator heater. The gas stream is expanded to supersonic speeds through an interchangeable, water-cooled facility nozzle. For the experiments of this work, a Mach 2.7 nozzle is used. The gas passes through a water-cooled facility isolator which serves to contain the pre-combustion pressure rise. Liquid JP-7 fuel is heated to a vaporized condition and injected to the near atmospheric pressure gases just upstream of a cavity-based flameholder.

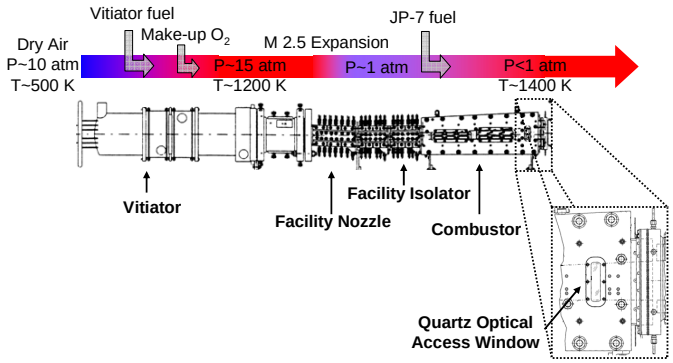

Figure 2. Schematic of WPAFB scramjet test rig.

The combustor is fitted with 2.5 cm x 12 cm quartz optical access ports. An enlarged view of the optical access ports used for this work is inset in Fig. 2. The ports are located 16.5 cm upstream of the end of the combustor. The outward face of each window is wedged to avoid optical interference effects which arise when scanning laser wavelength in the presence of parallel optical faces in the beam path. The collimating pitch and catch optics are arranged on translation stages that can vertically traverse the optical ports while maintaining beam alignment. The optics are positioned six inches from the access ports to avoid thermal damage and the open beam path between the optics and the windows is enclosed by open-ended tubes with a continuous nitrogen flow to eliminate interference from ambient water vapor.

C. Line Selection

All absorption spectroscopy techniques rely on careful selection of the quantum transitions (lines) that will be used to probe the gaseous flow. Careful selection begins by choosing transitions of a species present in the flow (in this case, water vapor) with desirable absorption properties for the particular application. For these experiments, three lines are chosen with different lower state energies. The lower state energy, E", determines the equilibrium molecular population in the un-excited state for a transition as a function of temperature, and thus can be used to describe how the absorption strength of a particular transition varies with temperature. A discussion of optimal line selection procedure can be found in Ref. 24. The three transitions used for these experiments are shown in Table 1. The lower state energies were chosen to give a peak temperature sensitivity for the 1392 nm and 1343 nm features at 500 K and the 1392 and 1469 nm features at 1600 K. These temperatures coincide with the expected temperature of a scramjet run with only the vitiator operating and with full combustion, respectively.

Wavelength *nm* (Hitran '04)	Frequency cm^{-1} (Hitran '04)	Line Strength (296 K) $cm^{-2}\,atm^{-1}$ (Hitran '04)	Line Strength (296 K) $cm^{-2}\,atm^{-1}$ (Measured)	Lower State Energy cm^{-1} (Hitran '04)
1392	7185.6	$1.97(10)^{-2}$	$1.96(10)^{-2}$	1045.1
1343	7444.35 and 7444.37	$1.12(10)^{-3}$	$1.10(10)^{-3}$	1774.8 and 1806.7
1469	6807.83	$1.02(10)^{-6}$	$6.48(10)^{-7}$	3319.4

Table 1. Line strength and lower state energy parameters for spectroscopic features used in these experiments.

The three lines were also chosen for their isolation from other transitions, laser availability, and correct wavelength spacing to allow dispersal by the grating. The key spectral parameter of line strength was validated for each feature under carefully controlled conditions in a laboratory furnace.

D. Measurement Techniques

1. Scanned-Wavelength Direct Absorption

Scanned-wavelength direct absorption has been a staple of TDL sensors for harsh environments. The important aspects of the technique are shown in Fig. 3. The injection current of the TDL is driven with a linear ramp signal (in this case, a 4 kHz sawtooth signal). The linear ramp in injection current results in a near-linear variation in laser intensity which can be seen in Fig. 3a. The variation in laser intensity is accompanied by a near-linear change in laser wavelength. As the laser is tuned across the absorption feature some light is absorbed, reducing the detector signal. A baseline fit is performed on the non-absorbing "wings" of the feature to infer the laser intensity in the absence of absorption. The Beer-Lambert relation (Eq. 1) can be rearranged to yield Eq. 2, which gives the absorbance (α) as a function of the transmitted laser intensity (I_t, the detector signal), and the incident laser intensity (I_o, the baseline fit). The absorbance plot resulting from the laser scan in Fig. 3a is shown in Fig. 3b.

$$\frac{I_t}{I_o} = \exp(-\alpha) \tag{1}$$

$$\alpha = -\ln\left(\frac{I_t}{I_o}\right) \tag{2}$$

The absorbance is a function of line strength (S), species partial pressure (P_i), pathlength (L), and line shape function (ϕ) as shown in Eq. 3.

$$\alpha = S(T) \times P_i \times L \times \phi(v) \tag{3}$$

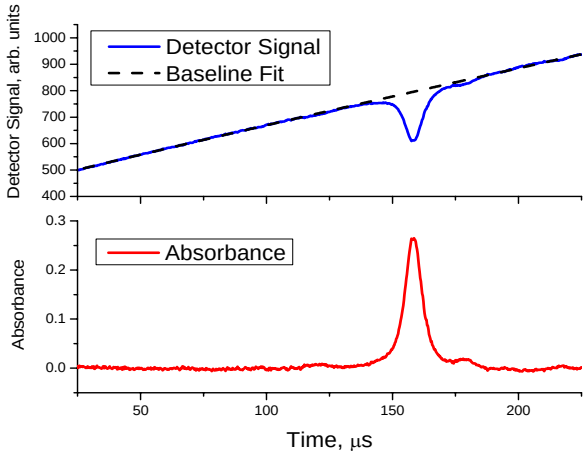

Figure 3a (top). Raw detector signal during a full combustion run for a single direct absorption laser scan with baseline fit (1392 nm feature)
Figure 3b (bottom). Absorbance plot resulting from laser scan and baseline.

The line shape is a normalized function that describes the profile of a spectroscopic transition in frequency space. Thus if the measured absorbance of a transition is fit with the proper profile (a Voigt profile is used here) and integrated with respect to frequency, the line shape function is equal to unity and is no longer important. This is shown in Eq. 4, where the result from integrating with respect to frequency is called the integrated absorbance area.

$$area = S(T) \times P_i \times L \times \int_{-\infty}^{\infty} \phi(v) \cdot dv = S(T) \times P_i \times L \tag{4}$$

For thermometry, the ratio of the integrated area of two absorption features is used. When the ratio is taken, the species partial pressure and pathlength cancel. The remaining ratio of line strengths is purely a function of temperature and is used to infer the temperature from the measured area ratio.

$$\frac{area_1}{area_2} = \frac{S_1(T)}{S_2(T)} \tag{5}$$

The species concentration is calculated using Eq. 4 with one spectral feature. The area and pathlength are known, and the line strength is calculated using the temperature previously inferred from the ratio.

2. Scanned-WMS-2f

The theory of WMS with 2*f* detection has been covered extensively in the literature.[10-18] It is generally used in situations involving small absorbances and/or noisy environments.[19-24] In its most basic form, WMS-2*f* involves rapidly modulating the laser wavelength, passing the light through an absorbing medium, and running the detector signal through a lock-in amplifier set to isolate the signal at twice the modulation frequency. The resulting signal can be used to calculate various gasdynamic properties. In the scanned-wavelength variant of WMS-2*f* employed

here, the rapidly modulated laser wavelength is also slowly tuned across an absorption feature and the peak height of the WMS-2*f* signal is used to infer gas properties. Fig. 4a depicts the raw detector signal of a single sweep of scanned-WMS-2*f*. As with the direct absorption method discussed before, the laser injection current is driven with a linear ramp (2 kHz), but now there is also a high frequency sinusoid superimposed on the ramp (190 kHz). The laser intensity varies with the drive signal, and is accompanied by a similar variation is laser wavelength.

The laser frequency (inverse wavelength), ν(t), and the laser intensity, $I_o(t)$, for the situation described above are given by Eq. 6 and 7.

$$\nu(t) = \bar{\nu}(t) + a\cos(\omega t) \tag{6}$$

$$I_o(t) = \bar{I}_o(t)[1 + i_o(t)\cos(\omega t + \psi)] \tag{7}$$

where $\bar{\nu}(t)$ and $\bar{I}_o(t)$ are the average laser frequency and intensity which are slowly varying due to the linear ramp, ω is the modulation frequency, a is the frequency modulation amplitude, and $i_o(t)$ is the intensity modulation amplitude (which is a constant normalized by $\bar{I}_o(t)$). ψ is the phase shift between frequency and intensity and is commonly assumed in the literature to be π[10,13]. Due to the small modulation depths utilized for this work, this assumption is made with minimal resulting error; however it should be noted that for real diode lasers ψ is somewhat greater than π and can be measured. The reader should also be aware that nonlinear terms in the intensity and frequency equations, which are neglected here, become important if large modulation depths are used.[18]

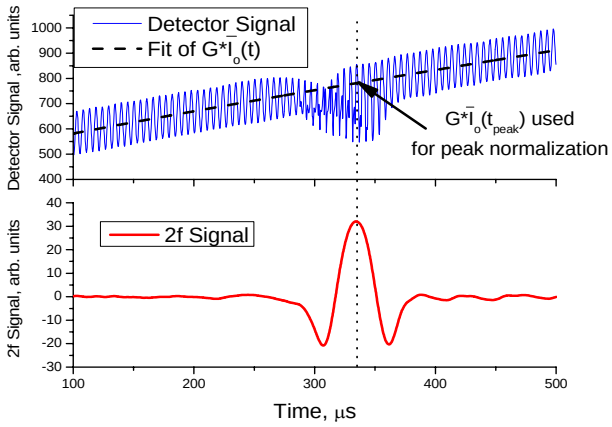

Figure 4a (top). Raw detector signal during a full combustion run for a single laser scan with modulation (1392 nm feature). Also shown is fit to obtain $G^*I_o(t)$. Figure 4b (bottom). WMS-2*f* signal resulting from laser scan.

When modulated laser light at a frequency corresponding to a quantum transition is passed through an absorbing medium, it is attenuated. The intensity of light that remains after having passed through the medium (I_t) is proportional to a transmission coefficient (τ) which is a function of the frequency of the light:

$$I_t(t) = I_o(t)\cdot\tau(\bar{\nu} + a\cos\omega t) \tag{8}$$

Because the transmission coefficient is a periodic, even function in ωt, it can be expanded in a Fourier cosine series:

$$\tau(\bar{\nu} + a\cos\omega t) = \sum_{k=0}^{\infty} H_k(\bar{\nu}, a)\cdot\cos(k\omega t) \tag{9}$$

$$where \quad H_o(\bar{\nu}, a) = \frac{1}{2\pi}\int_{-\pi}^{\pi}\tau(\bar{\nu} + a\cos\theta)d\theta \tag{10}$$

$$H_k(\bar{\nu}, a) = \frac{1}{\pi}\int_{-\pi}^{\pi}\tau(\bar{\nu} + a\cos\theta)\cos k\theta d\theta \tag{11}$$

Combining Eq. 8 and 9 gives the raw detector signal that is passed into the lock-in amplifier. The lock-in is set to isolate the second harmonic of the detector signal by multiplying the signal by a sinusoidal reference at twice the modulation frequency and low-pass filtering the results (thus retaining only the DC terms). The mathematical details will not be shown here but the resulting signal, normalized by the average laser intensity and detector gain ($G\bar{I}_o$) is given by Eq. 12. This equation assumes linear frequency and intensity modulation with a phase shift of π. Note that Eq.12 could be written as a function of time, however because the average laser frequency varies in time with the linear ramp, average laser frequency is analogous to time. It will be advantageous to have the WMS-2*f* signal in terms of average laser frequency for the purpose of comparing with simulations.

$$\frac{S_{2f}(\bar{\nu})}{G\bar{I}_o(\bar{\nu})} = \frac{1}{2}\left[H_2 + \frac{i_o(\bar{\nu})}{2}(H_1 + H_3)\right] \tag{12}$$

It is desirable to understand the lock-in amplifier output in terms of spectral parameters so that the measured signal can be used to calculate gas properties. The transmission coefficient at a specific frequency is also given by the Beer-Lambert relation, $\tau(v) = \exp(-S(T) \cdot P_i \cdot L \cdot \phi(v))$, which can be substituted into Eq. 11 to yield an equation for H_k in terms of spectral parameters. Note that the summation of the line strength and line shape accounts for overlapping spectral features.

$$H_k(\bar{v}, a) = \frac{1}{\pi} \int_{-\pi}^{\pi} \exp\left[- P_i \cdot L \cdot \sum_j (S_j(T) \cdot \phi_j(\bar{v} + a\cos\theta)) \right] \cos k\theta d\theta \tag{13}$$

If the contribution from neighboring spectral features is neglected and the signal at line center is gathered (i.e. WMS-2*f* peak height), the H_1 and H_3 terms of Eq. 12 can be neglected because they are odd functions about line center. In addition if the main feature is assumed to be optically thin (absorbance less than approximately 0.1), the Beer-Lambert relation can be linearized, $\tau(v) \approx 1 - (S(T) \cdot P_i \cdot L \cdot \phi(v))$, leaving the following simplified WMS-2f peak height equation:

$$\frac{S_{2f}(\bar{v}_{peak})}{G\bar{I}_o(\bar{v}_{peak})} = -\frac{S(T) \cdot P_i \cdot L}{2\pi} \int_{-\pi}^{\pi} \phi(\bar{v}_{peak} + a\cos\theta)\cos 2\theta d\theta \tag{14}$$

When taking the ratio of WMS-2*f* peak height signals from two spectral lines the partial pressure and pathlength cancel, leaving only the line shape integral and line strength for each line. Fortunately, the modulation depth of each laser can be chosen such that the line shape integral is nearly constant for moderate changes in pressure and mixture composition. This important point is discussed in detail by Liu *et al.*[10] Thus if WMS-2*f* peak height simulations are performed at the nominal expected partial pressure for both lines as a function of temperature, the resulting ratio of the two simulations will form a map between WMS-2*f* peak ratio and temperature. This map will be unaffected by moderate changes of mixture composition and pressure about the nominal value used for simulation.

To infer gas properties, the measured signals are compared with simulations. For temperature, the measured WMS-2*f* peak ratio is compared with the map described above. To calculate partial pressure of the species, the simulation for one spectral line (at the temperature inferred by the two line ratio) is ratioed with the measured peak height of that line. As shown in Eq. 14, the WMS-2*f* signal is directly proportional to the partial pressure of the species, so the ratio of the measured WMS-2*f* signal and the simulation will exactly equal the ratio of the measured partial pressure and the partial pressure used in simulation. This is shown in Eq. 15, which is arranged to obtain the measured partial pressure.

$$\frac{\left(\frac{S_{2f}(\bar{v}_{peak})}{G\bar{I}_o(\bar{v}_{peak})}\right)_{measured}}{\left(\frac{S_{2f}(\bar{v}_{peak})}{G\bar{I}_o(\bar{v}_{peak})}\right)_{simulated}} \cdot P_{H_2O,simulated} = P_{H_2O,measured} \tag{15}$$

Neglecting neighboring features and assuming optically thin transitions are key assumptions necessary to simplify the WMS-2*f* signal to show its functionality and dependence on gas properties and spectral parameters (Eq. 14). For the spectral features chosen for these experiments, however, there are small neighboring features that may contribute to the WMS-2*f* peak height. Also, in the case of the 1392 and 1343 nm features, the average peak absorbance is near 0.30 during a full combustion run, which is just outside the range that is normally regarded as optically thin. For these reasons, it is necessary to perform full simulations using Eq. 12 and Eq. 13, which do not make any assumptions, and check that the ratio of the WMS-2*f* peak height signals is sufficiently unaffected by variations in pressure and mixture composition. This is shown in Fig. 5. In Fig. 5a, simulations were performed for the 1392 and 1469 nm WMS-2*f* ratio at the mean measured pressure of a full combustion run, and again at the mean pressure ± 5% (a conservative value for the maximum pressure fluctuation during a full combustion run). The figure shows that if the simulation assuming the mean pressure is used to infer the temperature from the measured ratio, the measurement error if the actual pressure is within 5% of the mean pressure will be less than 5 K. In Fig. 5b, the process is repeated varying the H_2O mole fraction ± 10% of the expected nominal value. Thus even though the simplifying assumptions have been lifted in the simulations, the dependence of the WMS-2*f* peak ratio on pressure and mixture composition is negligible.

The method above yields absolute measurements of temperature and concentration so long as rough values of pressure and mole fraction are known. This is made possible by careful normalization of the WMS-2*f* peak height and the use of full simulations with judiciously chosen laser parameters (a, i_o).

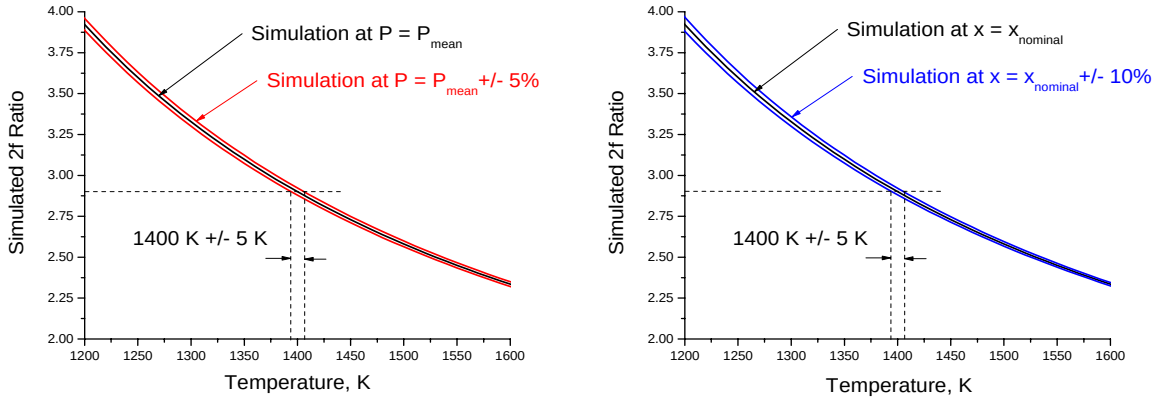

Figure 5a (left). Simulated WMS-2f ratio for the 1392nm / 1469 nm line pair at the mean pressure of a full combustion run. The light boundaries are simulations at ± 5% of the mean pressure, a conservative estimate of the maximum pressure fluctuation during a combustion run.
Figure 5b (right). Simulated WMS-2f ratio for the 1392nm / 1469 nm line pair at the nominal H_2O mole fraction during a combustion run. The light boundaries are simulations at ± 10% of the nominal mole fraction, a conservative estimate of the maximum mole fraction fluctuation during a run.

III. Comparison of Direct Absorption and WMS-2*f* Measurements

A. Influence of Noise

The scanned-wavelength direct absorption method works well in environments where spectrally-isolated features with large absorbances can be used and noise eliminated with optical engineering. However, as is the case with these and other applications to harsh flows, some level of noise will always be present and high temperatures will require the use of weakly absorbing features. WMS-2*f* offers certain advantages that can address these issues.

1. Baseline fitting

Baseline fitting is a key component of scanned-wavelength direct absorption data reduction, however several factors increase the difficulty of making a good fit. Fiber mode noise causes time and wavelength-dependent fluctuations that bend and distort the intensity ramp of the detector signal. Gasdynamic and mechanical beam steering causes signal fluctuations resulting in further errors. In the limit that optical engineering can control the aforementioned noise sources, a difficulty that is still present is interference from neighboring spectral features. Determining where baseline fits should begin and end to avoid the wings of the main and neighboring spectral features greatly exacerbates baseline fitting. This effect is apparent in Fig. 3 of section IID and especially shows for the 1343 and 1469 nm features in Fig. 6.

For small modulation depths, the WMS-2*f* signal in the absence of absorption is zero regardless of laser intensity. This means the WMS-2*f* signal rides on a zero background and does not depend on any baseline fitting. The reader may note in Eq. 12 that the measured WMS-2*f* peak height must be normalized by $G\bar{I}_o$ in order to compare with the simulations. To do this, a low order polynomial is fit through the high frequency modulation, as shown in Fig. 4a. While it may seem that an error in the fit through the WMS-2*f* signal would induce the same problems as an error in the baseline fit of a direct absorption scan, this is not true. There is a difference of relative measurement scales. As an example, a 1% error in the fit of $G\bar{I}_o$ used to normalize the WMS-2*f* signal will result in only a 1% error in the normalized WMS-2*f* peak height. However, since the absorbance is measured relative to the baseline fit of a direct absorption scan, a 1% error on the fit of a feature with 10% peak absorbance will cause 10% or more error. For this reason WMS-2*f* is less prone to baseline fitting errors than direct absorption.

2. Detection bandwidth

With direct absorption spectroscopy one must rely entirely on optical engineering to reduce noise. WMS-2*f*, however, employs the use of a lock-in amplifier which serves to shift the detection bandwidth above most noise sources. The lock-in amplifier multiplies the detector signal by a sinusoidal reference wave at twice the modulation frequency. In doing this, the components of the detector signal at all frequencies are shifted in frequency space such that the signal at twice the modulation frequency becomes a DC signal. The entire signal is then low-pass filtered to eliminate the shifted signals outside of the low pass filter cutoff, thereby eliminating nearly all but the signal at twice the modulation frequency. For the experiments presented here, the modulation frequency is 190 kHz. The lock-in amplifier multiplies the detector signal by a 380 kHz sine wave and then low-pass filters the result with a 75 kHz cutoff, 8th order IIR cascade filter. The resulting signal thus only contains signals that were originally at 380 kHz +/- 75 kHz. Because most noise sources are below 300 kHz (including 1/*f* laser noise), they are filtered out and do not contribute to the final signal.

B. Comparison of Direct Absorption and WMS-2*f* Results

This section will compare results obtained in the scramjet engine with both direct absorption and WMS-2*f* to illustrate the differences described earlier. For each comparison, the data was taken on consecutive runs of the scramjet under the same conditions.

Figure 6 shows an example scan for each line obtained during a full combustion run with both methods. The top panel shows absorbance data which come from fitting a baseline to the raw laser scan. One can see the neighboring features which reduce the percentage of each scan that can be fit with the critical zero absorption baseline. Also, the features overlap, complicating Voigt fitting and the determination of the integrated absorbance area. The bottom panel shows the WMS-2*f* data under the same scramjet conditions. The neighboring features appear as perturbations next to the main feature (which are not factored into the SNR). These features do not affect the measurement of the peak height however, because the zero baseline of the WMS-2*f* signal is inherent and does not come from a baseline fit. The contribution of the neighboring features to the WMS-2*f* peak height is small and accounted for by the simulations. Comparison of the SNR for each feature shows the improvements possible with WMS-2*f*. The SNR for the high temperature 1469 nm feature is improved by a factor of two.

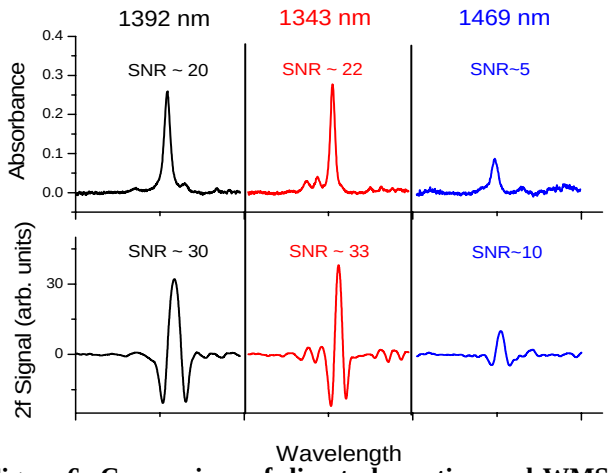

Figure 6. Comparison of direct absorption and WMS-2f signals during a full combustion run.

Figure 7 shows a comparison of the measured temperature using the 1392/1469 nm line pair with direct absorption and WMS-2*f*. The WMS-2*f* data has a 2 kHz sampling rate (1 WMS-2*f* peak per laser scan at 2 kHz), so the direct absorption data was filtered to 2 kHz from its original 4 kHz sampling rate to give a fair comparison. The figure shows an improvement in the standard deviation of the temperature fluctuations from 90 K to 50 K.

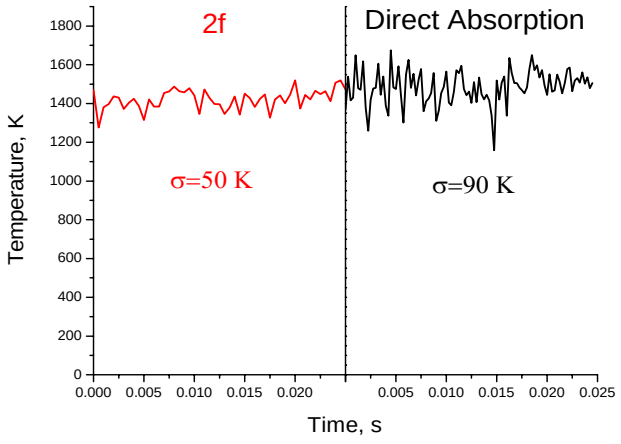

Figure 7. Comparison of measured temperature using direct absorption and WMS-2*f* with the 1392/1469 nm line pair. The direct absorption data was filtered from 4 kHz to 2 kHz to match the WMS-2f sampling rate. ϕ = 1.02.

Figure 8 is a comparison of FFTs of the temperature data obtained with each method. Frequency modes at 20, 60, and 120 Hz can clearly

be seen in the FFT of the direct absorption data. None of these modes are present in the WMS-2*f* data. This suggests that the frequency modes in the direct absorption data are not fluctuations in the actual gas temperature of the scramjet, but rather fluctuations in the inferred temperature due to mechanical or electrical noise sources that affect the direct absorption signal. These noise sources do not appear in the WMS-2*f* signal because they are filtered out by the lock-in amplifier. Note that should there be frequency modes in the fluctuations of the actual gas temperature of the scramjet (pattern factors), they would still appear in the WMS-2*f* FFT.

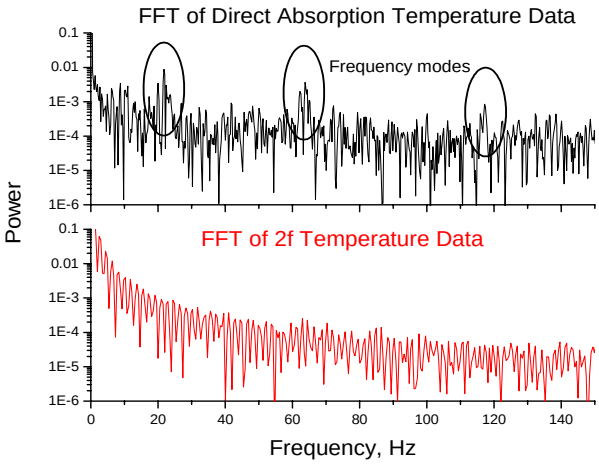

Figure 8. Comparison of FFT power spectrum obtained from direct absorption and WMS-2*f* temperature measurements (normalized power).

IV. Demonstration of Sensor Potential

This section will give some examples of the useful information that the sensor can yield. The data for all figures of this section were acquired with WMS-2*f* and are shown at the full 2 kHz sampling rate.

Figure 9 shows 0.75 seconds of representative temperature and H_2O partial pressure data. A portion of the start-up transient of the scramjet combustor is shown. The mean temperature increases for approximately 0.45 seconds before stabilizing, while the mean H_2O partial pressure remains stable throughout. These data can be used to characterize transients in the scramjet that may be difficult to predict with models.

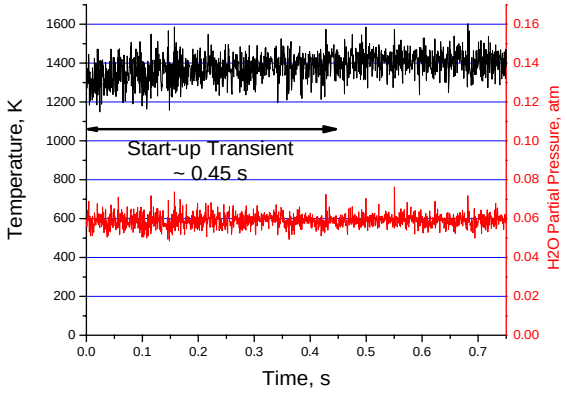

Figure 9. Temperature and water concentration data obtained with WMS-2*f* showing a portion of the start-up transient after combustor ignition. 1392/1469 nm line pair. ϕ = 1.20.

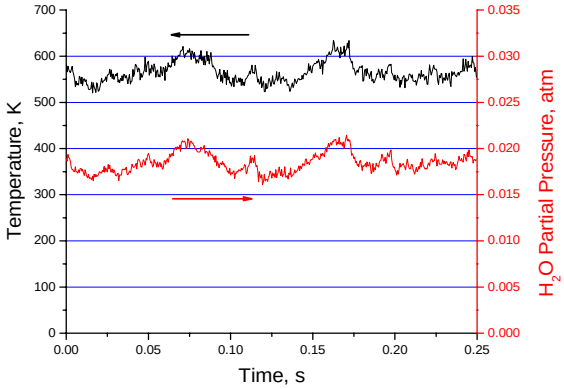

Figure 10. Temperature and water concentration with only the vitiator running (no combustor). 1392/1343 nm line pair.

Figure 10 shows temperature and water partial pressure with only the vitiated heater. The 1392/1343 nm line pair was used because this pair offers good temperature sensitivity at these conditions. These data are useful to characterize vitiator performance and further demonstrate the responsiveness of the sensor to transients.

Figure 11 shows measurements of mean temperature as a function of fuel/air equivalence ratio using the 1392/1469 nm line pair. The error bars represent a single standard deviation of the data at 2 kHz. Also shown is the temperature calculated by a 1-D model developed by the researchers at Wright-Patterson AFB. The model solves the 1-D conservation equations incorporating reactant mass flow rate, load cell force, heat loss, and pressure data from each run. Some deviation between the simulated and measured temperatures is expected because the model predicts the temperature at the end of the combustor, which is 16.5 cm downstream from the measurement location. Two competing phenomena occur in the scramjet between the measurement location and the end of the combustor; the duct diverges, causing pressure drop and a corresponding temperature drop, and heat release may still be occurring as the gases pass the measurement location, which will cause an increase in temperature. Another factor to consider is that the beam path for the laser measurements may be positioned at an elevation that is not representative of the 1-D temperature. The key aspect of Fig. 11 is that the trend of the measured temperature matches that of the simulated temperature. Measurements of this nature are helpful to determine optimal scramjet run parameters such as fuel/air ratio or to characterize the efficiency of various flameholder designs or engine components.

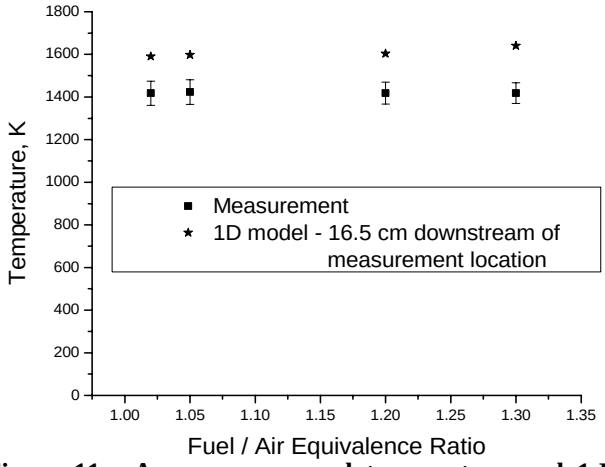

Figure 11. Average measured temperature and 1-D simulated temperature (6.5 inches downstream of measurement location) versus combustor fuel/air equivalence ratio. Error bars represent standard deviation at 2 kHz sample rate. 1392/1469 nm line pair.

V. Conclusions

Diode laser sensors provide an excellent means to measure gas temperature and species concentration in harsh environments. Scanned-wavelength direct absorption spectroscopy is often used because of its simplicity and ability to make absolute measurements. Scanned-WMS-2*f* offers reduced sensitivity to baseline fitting and increased noise rejection over direct absorption, but is often used for relative measurements which require a calibration. Through proper normalization of the signal and comparison with simulations, absolute measurements may be made.

A fiber-coupled, four-wavelength system with a grating-based demultiplexer provides a rugged, portable means to make measurements on the scramjet test rig at Wright-Patterson AFB. Careful optical engineering helps reduce mechanical and gasdynamic beam steering and fiber mode noise effects. Both scanned-wavelength direct absorption and scanned-WMS-2*f* are performed in the scramjet test rig. The results show an increase in SNR for WMS-2*f* over direct absorption, and the ability of WMS-2*f* to reject noise outside the lock-in amplifier bandwidth. The results also show the usefulness of the sensor to detect transients and as a means to validate models and optimize running parameters of the engine.

Acknowledgments

This research was sponsored by the Air Force Office of Scientific Research (AFOSR), Aerospace and Materials Science Directorate, with Dr. Julian Tishkoff as technical monitor.

References

[1]R.K. Hanson and J.B. Jeffries, "Advances in Laser-Based Sensors for Propulsion Systems," *24th AIAA Aerodynamic Measurement Technology and Ground Testing Conference*, AIAA-2004-2476, Portland, Oregon, June 28-1, 2004.

[2]S.T. Sanders, J.A. Baldwin, T.P. Jenkins, D.S. Baer, and R.K. Hanson, "Diode-laser sensor for monitoring multiple combustion parameters in pulse detonation engines," *Proceedings of the Combustion Institute* 28, 2000, pp. 587-594.

[3]M.G. Allen, "Diode laser absorption sensors for gas-dynamic and combustion flows," *Meas. Sci. Technol.* 9**,** 1998, pp. 545-562.

[4]J.T.C. Liu, J.B. Jeffries, R.K. Hanson, S. Creighton, J.A. Lovett, D.T. Shouse, "Diode Laser Absorption Diagnostics for Measurements in Practical Combustion Flow Fields," *39th AIAA/ASME/SAE/ASEE Joint Propulsion Conference*, AIAA-2003-4581, Huntsville, Alabama, July 20-23, 2003.

[5]J.T.C. Liu, G.B. Rieker, J.B. Jeffries, R.K. Hanson, M.R. Gruber, C.D. Carter, and T. Marthur, "Near-infrared diode laser absorption diagnostic for temperature and water vapor in a scramjet combustor," *Applied Optics*, in press 2005.

[6]R.A. Baurle, T. Marthur, M.R. Gruber, and K.R. Jackson, "A numerical and experimental investigation of a scramjet combustor for hypersonic missile applications," *34th AIAA/ASME/SAE/ASEE Joint Propulsion Conference*, AIAA-1998-3121, Cleveland, Ohio, July 13-15, 1998.

[7]M. Gruber, J. Donbar, K. Jackson, T. Marthur, R. Baurle, D. Eklund, and C. Smith, "Newly developed direct-connect high-enthalpy supersonic combustion research facility," *Journal of Propulsion and Power* 17, 2001, pp, 1296-1304.

[8]T. Mathur, M.R. Gruber, K.R. Jackson, J. Donbar, W. Donaldson, T. Jackson, C. Smith, and F. Billig, "Supersonic combustion experiments with a cavity-based fuel injector," *Journal of Propulsion and Power* 17, 2001, pp. 1305-1312.

[9]M.R. Gruber, K.R. Jackson, T. Marthur, and F. Billig, "Experiments with a cavity-based fuel injector for scramjet applications," ISABE paper IS-7154, September 1999.

[10]J.T.C. Liu, J.B. Jeffries, and R.K. Hanson, "Wavelength modulation absorption spectroscopy with 2*f* detection using multiplexed diode lasers for rapid temperature measurements in gaseous flows," *Applied Physics B* 78, 2004, pp. 503-511.

[11]R. Arndt, "Analytical line shapes for Lorentzian signals broadened by modulation," *J. Appl. Phys.* 36, 1965, pp. 2522-2524.

[12]J. Reid and D. Labrie, "Second-harmonic detection with tunable diode lasers – comparison of experiment and theory," *Applied Physics B* 26, 1981, pp. 203-210.

[13]L.C. Philippe and R.K. Hanson, "Laser diode wavelength-modulation spectroscopy for simultaneous measurement of temperature, pressure, and velocity in shock-heated oxygen flows," *Applied Optics* 32, 1993, pp. 6090-6103.

[14]P. Kluczynski, A. Lindberg, and O. Axner, "Background signals in wavelength-modulation spectrometry with frequency-doubled diode-laser light. I. Theory," *Applied Optics* 40, 2001, pp. 783-793.

[15]P. Kluczynski, A. Lindberg, and O. Axner, "Background signals in wavelength-modulation spectrometry with frequency-doubled diode-laser light. II. Experiment," *Applied Optics* 40, 2001, pp. 794-804.

[16]S. Schilt, L. Thevenaz, and P. Robert, "Wavelength modulation spectroscopy: combined frequency and intensity laser modulation," *Applied Optics* 42, 2003, pp. 6728-6738.

[17]P. Kluczynski and O. Axner, "Theoretical description based on Fourier analysis of wavelength-modulation spectrometry in terms of analytical and background signals," *Applied Optics* 38, 1999, pp. 5803-5815.

[18]H. Li, G.B. Rieker, X. Liu, J.B. Jeffries, and R.K. Hanson, "Extension of wavelength modulation spectroscopy to large modulation depth for diode laser absorption measurements in high-pressure gases," *Applied Optics*, submitted 2005.

[19]D.T. Cassidy and J. Reid, "Atmospheric pressure monitoring of trace gases using tunable diode lasers," *Applied Optics* 21, 1982, pp. 1185-1190.

[20]D.T. Cassidy and L.J. Bonnell, "Trace gas detection with short-external-cavity InGaAsP diode laser transmitter modules operating at 1.58 μm," *Applied Optics* 27, 1988, pp. 2688-2693.

[21]D.S. Bomse, A.S. Stanton, and J.A. Silver, "Frequency modulation and wavelength modulation spectroscopies: comparison of experimental methods using a lead-salt diode laser," *Applied Optics* 31, 1992, pp. 718-731.

[22]J.A. Silver and D.J. Kane, "Diode laser measurements of concentration and temperature in microgravity combustion," *Measurement Science Technology* 10, 1999, pp. 845-852.

[23]J. Wang, M. Maiorov, D.S. Baer, D.Z. Garbuzov, J.C. Connolly, and R.K. Hanson, "In situ combustion measurements of CO with diode-laser absorption near 2.3 μm," *Applied Optics* 39, 2000, pp. 5579-5589.

[24]X. Zhou, X. Liu, J.B. Jeffries, and R.K. Hanson, "Development of a sensor for temperature and water concentration in combustion gases using a single tunable diode laser," *Measurement Science Technology* 14, 2003, pp. 1459-1468.